Interoperability of the Voltage/Current Doubler Converter Employing Bipolar Pads with the SAE J2954 VA WPT2/Z2 for EV Wireless Charging

Grazian, Francesca; Soeiro, Thiago Batista; Bauer, Pavol

DOI
10.1109/PEMC51159.2022.9962951

Publication date
2022

Document Version
Final published version

Published in
Proceedings of the 2022 IEEE 20th International Power Electronics and Motion Control Conference (PEMC)

Interoperability of the Voltage/Current Doubler Converter Employing Bipolar Pads with the SAE J2954 VA WPT2/Z2 for EV Wireless Charging

Francesca Grazian
Dept. Electrical Sustainable Energy
Delft University of Technology
Delft, The Netherlands
F.Grazian@tudelft.nl

Thiago Batista Soeiro
Dept. Electrical Sustainable Energy
Delft University of Technology
Delft, The Netherlands
tbsoeiro@gmail.com

Pavol Bauer
Dept. Electrical Sustainable Energy
Delft University of Technology
Delft, The Netherlands
P.Bauer@tudelft.nl

2022 IEEE 20th International Power Electronics and Motion Control Conference (PEMC) | 978-1-6654-9681-0/22/$31.00 ©2022 IEEE | DOI: 10.1109/PEMC51159.2022.9962951

***Abstract*—This paper investigates the interoperability of the proposed voltage/current doubler (V/I-D) converter used for wireless charging of electric vehicles (EVs), which achieves high efficiency when charging both 400V and 800V batteries at the same power. Nominally, the V/I-D converter employs bipolar pads (BPP) at both the primary and the secondary circuits. In this study, the functionality of the converter is assessed when the primary BPP is coupled with a standard secondary coil, here being the VA test station WPT2/Z2 from SAE J2954. First, the intended operation of the V/I-D converter is explained. After that, the equivalent circuit of the BPP primary coupled with the standardized secondary coil is modeled analytically. The operation based on the misalignment is discussed. Then, the interoperability is verified through experimental results for the entire constant current charging mode for a rated output power of 7.2kW. Even though the functionality of the V/I-D converter is not optimal during the interoperability, the measured DC-to-DC power transfer efficiency in the considered operating range reaches the maximum at 95.22%, while the minimum is 92.86%.**

***Index Terms*—Battery voltage, bipolar pads, compensation networks, cross-coupling, electric vehicles, inductive power transfer, interoperability, rectangular coils, wireless charging.**

I. Introduction

Inductive power transfer (IPT) with magnetic resonance coupling has the potential to speed up the transition to electric vehicles (EVs) since it enables a user-friendly charging option: wireless charging. Especially when considering public parking infrastructures, it is important to ensure that EVs with different nominal battery voltages can be charged efficiently at the same power level. At the current date, the most common battery voltage ratings are $400\,\mathrm{V}$ and $800\,\mathrm{V}$ [1]. The proposed voltage/current doubler (V/I-D) converter shown in Fig. 1 is a universal solution to charge efficiently at the same power level both battery voltage classes. The power transfer control is executed only at the primary side through the modulation of the H-bridge inverters. Hereby, there is no need for a DC/DC converter connected to the battery, which simplifies the EV onboard circuit. This system requires two sets of coupled coils, here being bipolar pads (BPPs).

The BPP consists of two independent partially-overlapped rectangular coils. It was first introduced in [2] to implement a versatile EV transmitting pad that, depending on the direction of the current flowing through each coil, can work as a polarized or nonpolarized pad. Consequently, the BPP has high interoperability since it has relatively strong magnetic coupling with polarized pads such as double-D pads (DDPs) and nonpolarized pads such as circular or rectangular pads. Other examples of the BPP employed as a transmitting pad for interoperability can be found in [3]–[7]. Considering the V/I-D converter in Fig. 1, it is interesting to assess the functionality of the system when the secondary coil is not the intended BPP.

This paper explores the interoperability of the V/I-D converter when the primary BPP is coupled to a standardized rectangular secondary coil, here being the vehicle assembly (VA) test station WPT2/Z2 from SAE J2954 [8]. This is important because it makes the proposed converter applicable to more EVs. The functionality and properties of the V/I-D converter are explained in Section II. The interoperability is discussed in detail in Section III starting from the equivalent circuit modeling. After that, the operating scheme is analyzed depending on the misalignment. The analysis is proved with experimental results at the output power of $7.2\,\mathrm{kW}$ for the entire constant current (CC) charging mode. Finally, the main conclusion are given in Section IV.

II. V/I-D converter

A. Intended operation

The V/I-D converter has two operating modes depending on the nominal EV battery voltage, which is assumed to be either $400\,\mathrm{V}$ or $800\,\mathrm{V}$.

When the half-bridge legs with mid-point A and C in Fig. 1 are synchronized operating at 50% duty cycle as illustrated in Fig. 2(a), the current through the secondary coils has the same direction and, consequently, L_3 and L_4 result in a series connection. In the rectification stage, only D1 and D6 conduct during the positive half-wave of v_{ac}, while D3 and D4 conduct in the negative one. Since the two secondary coils conduct the same nominal current, this modulation is suitable for the voltage doubler mode, i.e., for $800\,\mathrm{V}$ batteries.

On the other hand, when the half-bridge legs with mid-point A and D in Fig. 1 have the same synchronized modulation as shown in Fig. 2(b), the current through the secondary coils has an opposite direction and, consequently, L_3 and L_4 result in a parallel connection. In this case, D1, D3, and D5 conduct

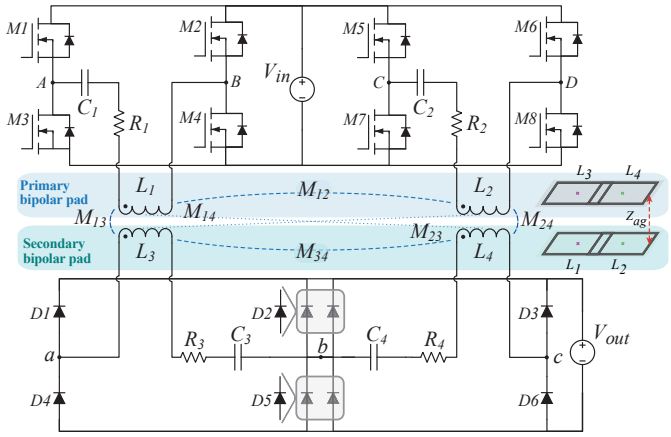

Fig. 1. V/I-D converter for IPT systems employing series-compensated BPPs.

during the positive half-wave of v_{ab} while D2, D4, and D6 conduct during the negative one. As illustrated in Fig. 2, each of the secondary coils still conducts the same nominal current as in the previous modulation, but their parallel connection results in double the load current. For the same output power P_{out}, this modulation is suitable for the current doubler mode, i.e., for 400 V batteries.

The key advantage of the proposed V/I-D converter is that the components have the same conduction losses in the two operating modes since they ideally conduct the same current. However, since two more diodes are conducting in the current doubler mode, the efficiency would be slightly lower than in the voltage doubler mode.

B. Coupled BPPs

The ideal operation of the V/I-D converter shown in Fig. 2 would be achieved if the cross-coupling between the BPPs is negligible, i.e., $M_{12} \approx M_{34} \approx M_{14} \approx M_{23} \approx 0$. However, when considering a pair of coupled BPPs, it is not possible to eliminate all the cross-coupling at the same time.

The two coils in the same BPP can be magnetically decoupled by appropriately selecting their overlap such that their concatenated magnetic flux approximates zero, achieving $M_{12} \approx M_{34} \approx 0$. This property is desirable when a BPP must be coupled with both rectangular pads and DDPs. As explained in [9], this overlapping area depends on the structure of the BPP itself and also on the configuration of the pad with which the BPP is coupled. Therefore, the overlapping area is generally chosen from the analysis of the pads through the finite element method (FEM).

However, when the BPPs are used as both the transmitting and receiving pads, the cross-coupling between the coils placed at the diagonal opposite sides of the circuit is present. Referring to Fig. 1, this cross-coupling is denoted by M_{14} and M_{23}. In [10], it has been shown that it is possible to minimize this diagonal cross-coupling by enlarging the overlapping area at the cost of reintroducing the cross-coupling between the coils on the same BPP. It is beneficial to eliminate the diagonal cross-coupling since it directly influences the power transfer from the primary to the secondary circuits. Moreover, as shown

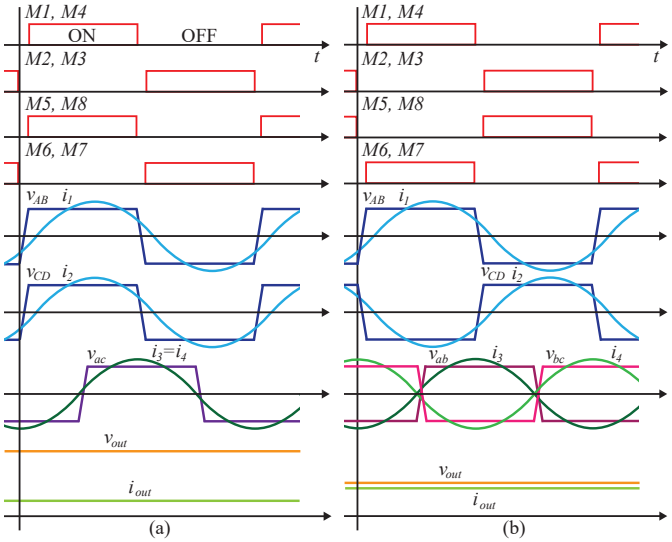

Fig. 2. Typical waveforms of the V/I-D converter operating as: (a) voltage doubler, and (b) current doubler.

TABLE I
CIRCUIT PARAMETERS OF THE V/I-D CONVERTER WITH COUPLED BPPS AT THE ALIGNED CONDITION. THE BPPS' OUTER DIMENSIONS AND THEIR AIR GAP ARE INCLUDED.

	L (μH)	R (mΩ)	M (μH)			(mm)
L_1	252.5	620	M_{13}	M_{12}	M_{14}	length x height
L_2	250.4	600	80.3	30.1	5.6	570 x 370
L_3	167.0	520	M_{24}	M_{34}	M_{23}	air gap
L_4	161.8	500	76.8	17.7	6.7	95

Ferrite: 3C95, PLT43/28/4.1 Litz wire: 600x0.072mm

(C_1, C_2, C_3, C_4) = (14.9, 14.9, 20.7, 21.6) nF $\rightarrow$ 4x(18,18,25,26)*

*(series x parallel): KEMET R76TF13305050J 3.3 nF (ESR=0.22 Ω)

in [11] and [12], the cross-coupling on the same BPP, i.e., M_{12} and M_{34} is relatively constant over the misalignment, which means that its effect could be compensated by adding extra compensation capacitance in the resonant circuit [12]–[14].

For the above-mentioned advantages, the design of the coupled BPPs with $M_{14} \approx M_{23} \approx 0$ has been chosen for the V/I-D converter. The circuit parameters at the aligned coils' conditions are summarized in Table I. Thereby, the outer dimensions of the BPPs and their air gap are also included. When the coupled BPPs are aligned, the measured DC-to-DC power transfer efficiency resulted in 96.53% at 800 V, and 96.34% at 400 V for an output power of 7.2 kW. These results follows from the intended operation of the V/I-D converter and they were achieved from a previous research on this topic.

III. INTEROPERABILITY OF THE PRIMARY BPP WITH THE TEST STATION VA WP2/Z2 FROM SAE J2954

The focus of this paper is assessing the performance of the V/I-D converter when it is not working in its nominal condition. For instance, it is considered that the primary BPP is coupled to a standardized secondary coil, resulting in the circuit schematic shown in Fig. 3.

A. Circuit and analytical modeling

The equivalent circuit in the frequency domain is shown in Fig. 4 where the EV battery is replaced by the equivalent

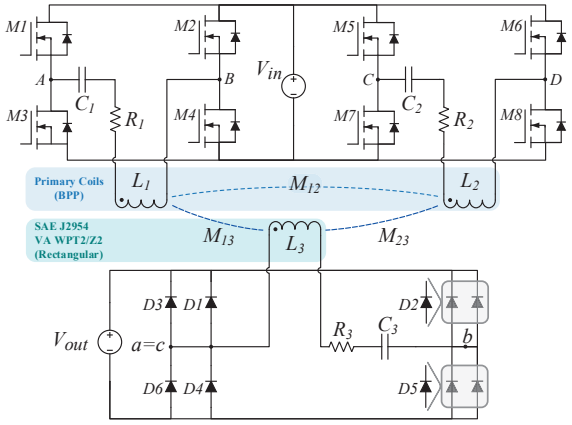

Fig. 3. Equivalent circuit of the V/I-D converter when coupled with the standard receiving coil SAE J2954 VA WP2/Z2.

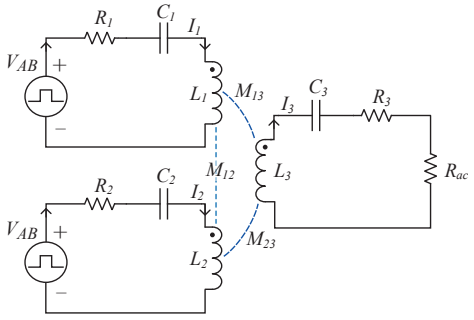

Fig. 4. Equivalent circuit in the frequency domain for analyzing the interoperability of the V/I-D converter in Fig. 3.

first-harmonic load R_{ac} in (1) defined by [15] and [16].

$$R_{ac} = \frac{8}{\pi^2} R_L = \frac{8}{\pi^2} \frac{V_{out}^2}{P_{out}} \tag{1}$$

The equivalent circuit in Fig. 4 is described by the Kirchhoff voltage law (KVL) in (2). Thereby, the impedance $\boldsymbol{Z_i}$ of each resonant circuit is defined in (3), and the mutual inductances M_{12}, M_{13}, M_{23} are expressed in (4). The input $\boldsymbol{V_{AB}}$ is taken as the reference according to the phasor convention, which is defined in (5) through the first-harmonic approximation, where V_{in} is the DC input voltage .

$$\begin{cases} \boldsymbol{V_{AB}} = \boldsymbol{Z_1 I_1} + j\omega M_{12} \boldsymbol{I_2} + j\omega M_{13} \boldsymbol{I_3} \\ \boldsymbol{V_{AB}} = j\omega M_{12} \boldsymbol{I_1} + \boldsymbol{Z_2 I_2} + j\omega M_{23} \boldsymbol{I_3} \\ 0 = j\omega M_{13} \boldsymbol{I_1} + j\omega M_{23} \boldsymbol{I_2} + (\boldsymbol{Z_3} + R_{ac}) \boldsymbol{I_3} \end{cases} \tag{2}$$

$$\boldsymbol{Z_i} = R_i + j\omega X_i, \quad X_i = \omega L_i - \frac{1}{\omega C_i} : \quad i = 1...4 \tag{3}$$

$$M_{ih} = M_{hi} = k_{ih} \sqrt{L_i L_h} : \quad i, h = 1...3 \wedge i \neq h \tag{4}$$

$$\boldsymbol{V_{AB}} = V_{AB,1} \angle 0° = \frac{4}{\pi} V_{in}, \quad V_{AB,1} = V_{CD,1} \tag{5}$$

Additionally, for a given processed power, the V/I-D resonant circuit's efficiency η_{res} is defined in (6).

$$\eta_{res} = \frac{R_{ac} |\boldsymbol{I_3}|^2}{V_{AB} (|\operatorname{Re}[\boldsymbol{I_1}]| + |\operatorname{Re}[\boldsymbol{I_2}]|)} \tag{6}$$

The total DC-to-DC efficiency $\eta_{\text{DC-to-DC}}$ also takes into account the power losses of the inverting and rectifying stages.

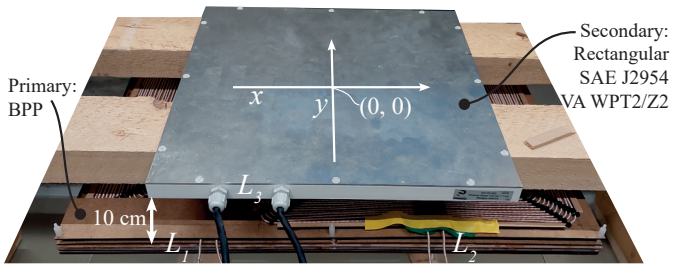

Fig. 5. Coupled coils configuration in the aligned position. Primary (L_1 and L_2): implemented BPP for the V/I-D converter. Secondary (L_3): commercial rectangular coil manufactured by PREMO [17].

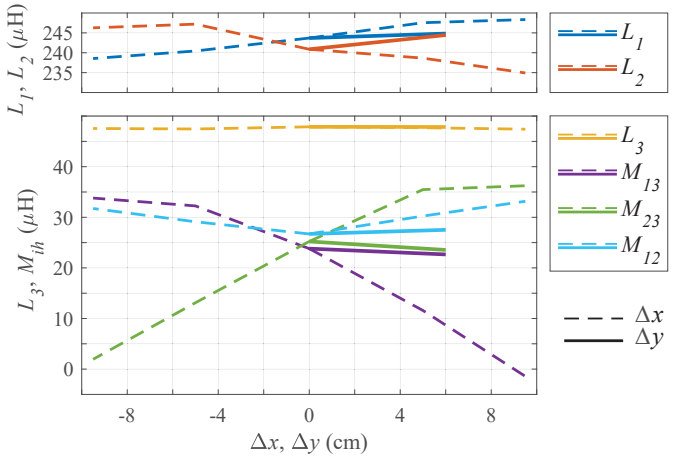

Fig. 6. Self-inductance and mutual inductance of the BPP primary coupled to the standardized secondary depending on the misalignment, which reference is shown in Fig. 5. Hereby, $i, h = 1...3 \wedge i \neq h$.

Assuming that $X_1 > 0$ and $X_2 > 0$, the H-bridge inverters operate in zero voltage switching (ZVS) turn-on losses, meaning that the power losses can be expressed as

$$P_{inv} = 4 \cdot R_{ds,on} \cdot \left[\left(\frac{I_1}{2} \right)^2 + \left(\frac{I_2}{2} \right)^2 \right] + \sum_{i=1}^{8} E_{off_{(Mi)}} \cdot f_0 \tag{7}$$

Additionally, since C_3 is chosen such that $X_3 \approx 0$, the rectifier's power losses are mainly due to the diodes' conduction:

$$P_{rect} = 8 \cdot \left[V_F \left(\frac{I_3}{\pi} \right) + r \left(\frac{I_3}{2} \right)^2 \right] \tag{8}$$

The parameters of the semiconductor devices can be extrapolated from their datasheet.

Finally, $\eta_{\text{DC-to-DC}}$ can be computed as

$$\eta_{\text{DC-to-DC}} = \eta_{res} \cdot \frac{P_{out}}{P_{out} + P_{inv} + P_{rec}} \tag{9}$$

B. Magnetic coupling and misalignment

Fig. 5 shows the magnetic arrangement in which the primary BPP is coupled to the WPT2/Z2 standard rectangular coil in the aligned position. The variations of the self-inductance and the mutual inductance depending on the misalignment are shown in Fig. 6.

When the two geometric centers are aligned, the secondary coil results in being misaligned in the x-direction with respect to both coils of the BPP. The movement along the x-axis

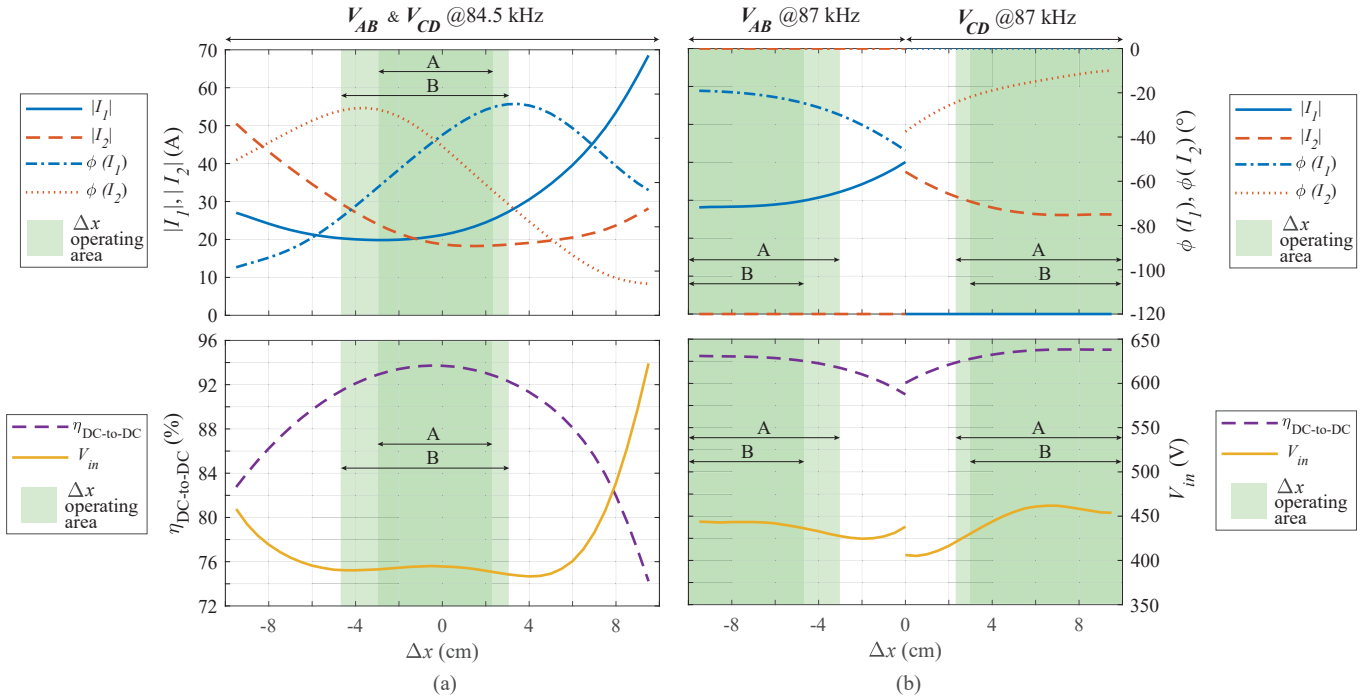

Fig. 7. Analysis of the absolute value and phase angle of the primary currents ($\boldsymbol{I_1}$, $\boldsymbol{I_2}$), the DC-to-DC efficiency $\eta_{\text{DC-to-DC}}$, and the required input voltage V_{in} depending on the receiving coil's misalignment in the x direction. The results suppose that a 400 V battery is charged at 7.2 kW. (a) Both H-bridge inverters are operated synchronously at 84.5 kHz, resulting in the two inverted voltages $\boldsymbol{V_{AB}}$ and $\boldsymbol{V_{CD}}$ being applied to the primary circuits. (b) Only one H-bridge inverter at the time is operated at 87 kHz. Specifically, $\boldsymbol{V_{AB}}$ drives the primary circuit when $\Delta x \leq 0$, while $\boldsymbol{V_{CD}}$ when $\Delta x \geq 0$. The shaded areas denote the preferred operating regions.

would improve the mutual inductance with respect to one of the primary coils, while the other one would worsen. On the other hand, the misalignment in only the y-direction causes a similar drop in M_{13} and M_{24}.

It is possible to notice that the mutual inductance between the two primary coils M_{12} is not negligible since its value might be comparable to M_{13} and M_{23}. This is due to the fact that, as explained in Section II-B, the coupled BPPs have been designed to minimize the diagonal cross-coupling between opposite coils while the effect of the cross-coupling within the same pad is balanced out through the compensation capacitors selection. Nevertheless, according to Fig. 6, M_{12} is not much dependent on the misalignment compared to M_{13} and M_{23}.

The current flowing through the two coils of the BPP must have the same direction such that the primary BPP assumes the character a of non-polarized pad which is preferable when coupled to a rectangular pad. This means that the H-bridge inverters must have the same modulation as in the voltage doubler switching scheme shown in Fig. 2(a). Considering that I_1 and I_2 have the same direction, the presence of M_{12} would push the primary currents further in the inductive region, preserving the ZVS turn-on of the MOSFETs. Therefore, M_{12} can be regarded as an extra positive reactance as shown by the KVL in (2). Nevertheless, based on the misalignment profile in Fig. 6, it is important to assess the operating conditions of the circuit in Fig. 3.

C. Operating conditions

1) Assumptions: Since the primary circuit stays unvaried, the value of both primary compensation capacitors results from the design of the V/I-D converter. For instance, C_1 and C_2 are the ones listed in Table I. Additionally, the compensation capacitance C_3=74.88 nF has been selected for the secondary rectangular coil.

The required input voltage V_{in} and the inverters' switching frequency must be selected such that the 400 V EV battery is supplied with the target output power of 7.2 kW, translating into a charging current of 18 A. Moreover, it must be guaranteed that both inverters operate in soft-switching. For these purposes, it is important to evaluate the operating points resulting from the measured self and mutual inductance conditions shown in Fig. 6. Hereby, it is assumed that:

- V_{in} can be set in the range 360...500 V that resembles the grid-connected boost-like power factor corrector (PFC) rectifier, which could be implemented as explained in [18] and [19];
- the operating frequency of the H-bridge inverters is constrained in the range allowed by SAE J2954, i.e., 79...90 kHz;
- the H-bridge inverters can be operated independently.

2) Analysis: Fig. 7 summarizes the resulting operating points depending on the misalignment in the x-direction which trend is shown in Fig. 5. Specifically, the parameters that have been computed from the analytical model of Section III-A are: the absolute value and phase angle of the primary currents $\boldsymbol{I_1}$ and $\boldsymbol{I_2}$, the DC-to-DC efficiency $\eta_{\text{DC-to-DC}}$, and the required V_{in} to achieve a charging current of 18 A while the battery voltage is 400 V. Two options are investigated, i.e., whether operating either the two H-bridge inverters synchronously or

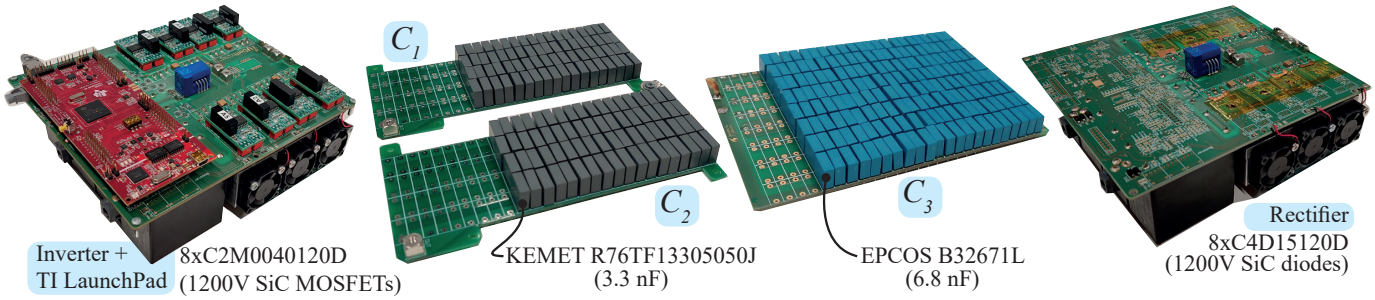

Fig. 8. Implemented inverter, rectifier and compensation networks with the relative devices.

only one at a time.

The results in Fig. 7(a) come as a consequence of operating both H-bridge inverters. The switching frequency of 84.5 kHz has been selected to ensure that the primary currents are inductive, i.e., they have a negative phase angle, to achieve the ZVS turn-on of the inverters while the required V_{in} is in the range covered by the PFC rectifier. When the receiver coil is placed in the aligned position (Δx=0), the current through the primary coils is relatively balanced and the maximum $\eta_{\text{DC-to-DC}}$ is expected. On the other hand, the misalignment along either the positive or the negative direction of the x-axis would improve the mutual inductance with respect to the more proximate primary coil while worsening the other. This translates into an exponential increase of the current in the primary coil with lower mutual inductance. This considerably increases the conduction losses in one of the primary circuits, resulting in the degradation of the total $\eta_{\text{DC-to-DC}}$ up to 20%. This is not acceptable according to the minimum efficiency requirements set by SAE J2954. Moreover, the winding of the primary coils is not rated to withstand such high current densities.

On the other hand, Fig. 7(b) shows the operating points resulting from the case in which only one H-bridge inverter is operated at the time. Specifically, $\boldsymbol{V_{AB}}$ drives the primary circuit when $\Delta x \leq 0$, while $\boldsymbol{V_{CD}}$ drives the primary circuit when $\Delta x \geq 0$. When the misalignment in the x-direction occurs, the coupling between the activated primary coil and the secondary coil increases. This lowers the current stress in the primary circuit for the same target output power resulting in higher power transfer efficiencies. This analysis takes into account that, by operating one primary coil at a time, the equivalent AC resistance of the primary coil is lower than in Fig. 7(a) since the proximity effect between the two primary coils becomes negligible. Additionally, it must be noted that, in this operating mode, the M_{12} does not contribute to the inductive behavior of the primary current. Therefore, when only one H-bridge inverter is operated, the switching frequency of the H-bridge inverter is increased to 87 kHz to ensure the ZVS turn-on of the inverter.

3) Selected operating strategy: One of the two operating modes in Fig. 7 would be selected to deliver power to the secondary coil depending on the coils' alignment. When the receiver coil is placed in the aligned position, it is preferable to use both H-bridge inverters to transfer the power to the load which results are shown in Fig. 7(a). This choice would limit the current density through the primary coils leading to the highest achievable efficiency. This is also valid when the receiver coil is misaligned in the y-direction since, according to Fig. 6, both M_{13} and M_{23} would drop proportionally. In that case, the output power would be regulated by controlling V_{in}. When the misalignment in the x-direction occurs over a certain threshold, only the primary coil with higher coupling to the secondary coil would be energized.

Examples of possible operating ranges are shown in Fig. 7 by the green-shaded areas denominated as A and B. Choosing the perimeter of A as the threshold between the two operating modes ensures that the $\eta_{\text{DC-to-DC}}$ is always maximum. On the other hand, the threshold can be selected based on other criteria such as the maximum allowed current stress through the primary coils to limit their temperature rise. This is the case for the operating area B which constraints the maximum peak current to 30 A.

D. Experimental results

To verify the interoperability of the V/I-D converter when the coupled coils consist of the ones in Fig. 5, the hardware in Fig. 8 has been used operating at the rated output power of 7.2 kW. The Delta Elektronika bidirectional power supplies SM500-CP-90 and SM1500-CP-30 are used as input and output voltage sources. The input power supply mimics the grid-connected boost-like PFC rectifier. The output power supply emulates the EV battery voltage for the whole CC charging mode. It is assumed that V_{in} is set according to the load, which information is given by the wireless communication required from the IPT system for several features such as guided positioning, pairing, and safety.

Fig. 9 shows the measured waveforms at different load and coils' alignment conditions together with the relative $\eta_{\text{DC-to-DC}}$. The measured $\eta_{\text{DC-to-DC}}$ and used V_{in} throughout the entire CC charging are plotted in Fig. 10 resulting from different coil's alignments.

1) Discussion: When the two geometric centers are aligned, the secondary coil is misaligned with respect to both primary coils causing higher primary currents for the same output power. This results in the measured $\eta_{\text{DC-to-DC}}$ being lower when the coils are aligned than when the secondary coil is misaligned along the x-axis. Additionally, the effect of M_{12} pushes the primary currents further into the inductive region worsening the turn-off losses of the H-bridge inverters. The highest $\eta_{\text{DC-to-DC}}$ has been measured when the L_3 is aligned

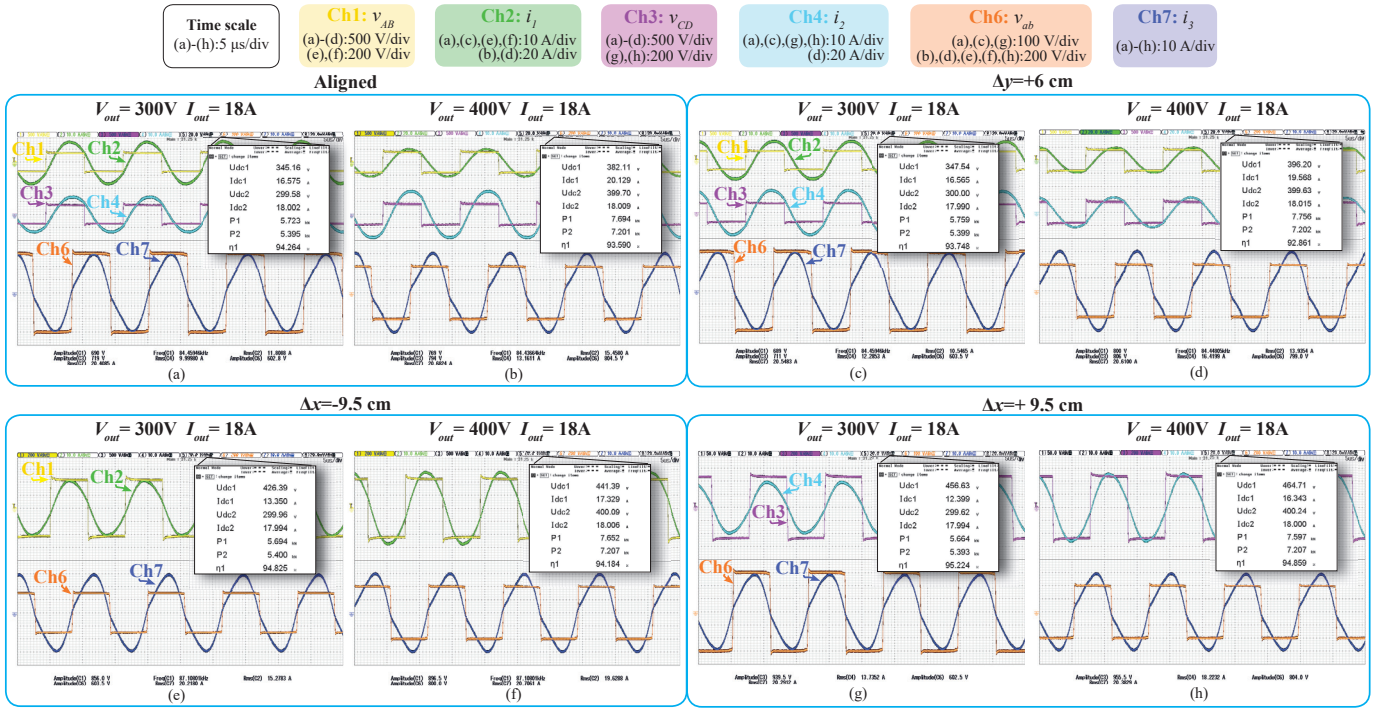

Fig. 9. Measured circuit waveforms at I_{out}=18 A together with the relative DC-to-DC power transfer efficiency at different coils' alignments where the reference axes are shown in Fig. 5. Aligned coils and V_{out}= (a) 300 V, (b) 400 V. Misalignment Δy=+6 cm and V_{out}= (c) 300 V, (d) 400 V. Misalignment Δx=-9.5 cm and V_{out}= (e) 300 V, (f) 400 V. Misalignment Δx=+9.5 cm and V_{out}= (g) 300 V, (h) 400 V.

with L_2 (Δx=9.5 cm) due to their shorter air gap, resulting in a lower input current for the same output power. For instance, efficiencies higher than 95% have been measured for most of that charging profile. Other two main factors contribute to the higher measured efficiency when only one H-bridge at a time is operated. One is the lower equivalent AC resistance of the primary coil since there is a great reduction of the proximity effect between the two primary coils. The other is the reduced turn-off power losses since the H-bridge inverter operates closer to the resonant frequency. Nevertheless, all the considered operating points are achieving the ZVS turn-on of the H-bridge inverters as shown in Fig. 9.

It must be also noted that, with this implementation, the current density of the primary coils is considerably higher than the intended from the nominal design with the coupled BPPs. This leads to a higher winding temperature and, consequently, higher resistance. If the primary BPP has to face interoperability, it is preferable to oversize the primary coils' Litz wire to reach an overall higher efficiency.

In the CC charging profile of Fig. 10, it is assumed that the battery voltage ranges from 300 V to 400 V. The utilized V_{in} mostly ranges from 360 V to 470 V which could be implemented in the European phase-to-neutral 230 V RMS network through a single-phase grid-connected PFC rectifier. Lower V_{in} values could be achieved by phase-shifting the inverters to decrease the fundamental component of $\boldsymbol{V}_{AB}$.

IV. Conclusion

The proposed V/I-D converter is a universal solution that achieves high power transfer efficiency for EV wireless charging of both 400 V and 800 V batteries at the same output power. This consists of two H-bridge inverters, series-compensated BPPs, and a rectification stage. This paper proves its interoperability when the primary BPP is coupled with a standardized rectangular coil, e.g., the VA test station WPT2/Z2 from SAE J2954. This is important because it enlarges the usability of the proposed converter. The analytical modeling and the intended operation have been discussed. Specifically, one or both H-bridge inverters are energized

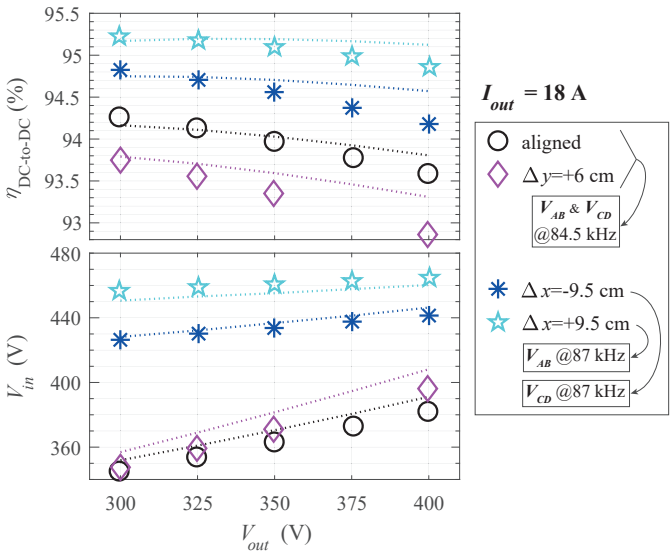

Fig. 10. Measured DC-to-DC efficiency $\eta_{\text{DC-to-DC}}$ and used input voltage V_{in} for the entire CC charging profile and at different coils' alignments. The dotted lines show the expected results from the analytical model in Section III-A.

depending on the coils' alignment. These conditions have been validated through experimental results for the whole CC charging mode and different alignments. The measured DC-to-DC efficiency ranges between 92.86% and 95.22%, which is relatively high considering that this is not the intended operation of the V/I-D converter.

REFERENCES

[1] "Voltage casses for electric mobility," ZVEI - German Electrical and Electronic Manufacturers' Association Centre, Tech. Rep., 2013. [Online]. Available: https://www.zvei.org/fileadmin/user_upload/Presse_und_Medien/Publikationen/2014/april/Voltage_Classes_for_Electric_Mobility/Voltage_Classes_for_Electric_Mobility.pdf

[2] G. A. Covic, M. L. G. Kissin, D. Kacprzak, N. Clausen, and H. Hao, "A bipolar primary pad topology for ev stationary charging and highway power by inductive coupling," in *2011 IEEE Energy Conversion Congress and Exposition*, 2011, pp. 1832–1838.

[3] A. Zaheer, H. Hao, G. A. Covic, and D. Kacprzak, "Investigation of multiple decoupled coil primary pad topologies in lumped ipt systems for interoperable electric vehicle charging," *IEEE Transactions on Power Electronics*, vol. 30, no. 4, pp. 1937–1955, 2015.

[4] F. Y. Lin, G. A. Covic, and J. T. Boys, "Evaluation of magnetic pad sizes and topologies for electric vehicle charging," *IEEE Transactions on Power Electronics*, vol. 30, no. 11, pp. 6391–6407, 2015.

[5] ——, "Leakage flux control of mismatched ipt systems," *IEEE Transactions on Transportation Electrification*, vol. 3, no. 2, pp. 474–487, 2017.

[6] F. Lin, G. A. Covic, and J. T. Boys, "A comparison of multi-coil pads in ipt systems for ev charging," in *2018 IEEE Energy Conversion Congress and Exposition (ECCE)*, 2018, pp. 105–112.

[7] F. Lin, G. A. Covic, and M. Kesler, "Design of a sae compliant multicoil ground assembly," *IEEE Journal of Emerging and Selected Topics in Industrial Electronics*, vol. 1, no. 1, pp. 14–25, 2020.

[8] *J2954 (R) Wireless Power Transfer for Light-Duty Plug-In/ Electric Vehicles and Alignment Methodology*, SAE International Std., Oct. 2020.

[9] A. Zaheer, D. Kacprzak, and G. A. Covic, "A bipolar receiver pad in a lumped ipt system for electric vehicle charging applications," in *2012 IEEE Energy Conversion Congress and Exposition (ECCE)*, 2012, pp. 283–290.

[10] H. Jafari, T. O. Olowu, M. Mahmoudi, and A. Sarwat, "Optimal design of ipt bipolar power pad for roadway-powered ev charging systems," *IEEE Canadian Journal of Electrical and Computer Engineering*, vol. 44, no. 3, pp. 350–355, 2021.

[11] W. Zhao, X. Qu, J. Lian, and C. K. Tse, "A family of hybrid ipt couplers with high tolerance to pad misalignment," *IEEE Transactions on Power Electronics*, vol. 37, no. 3, pp. 3617–3625, 2022.

[12] N. Rasekh, J. Kavianpour, and M. Mirsalim, "A novel integration method for a bipolar receiver pad using lcc compensation topology for wireless power transfer," *IEEE Transactions on Vehicular Technology*, vol. 67, no. 8, pp. 7419–7428, 2018.

[13] Y. Li, R. Mai, L. Lu, T. Lin, Y. Liu, and Z. He, "Analysis and transmitter currents decomposition based control for multiple overlapped transmitters based wpt systems considering cross couplings," *IEEE Transactions on Power Electronics*, vol. 33, no. 2, pp. 1829–1842, 2018.

[14] R. Mai, Y. Luo, B. Yang, Y. Song, S. Liu, and Z. He, "Decoupling circuit for automated guided vehicles ipt charging systems with dual receivers," *IEEE Transactions on Power Electronics*, vol. 35, no. 7, pp. 6652–6657, 2020.

[15] R. L. Steigerwald, "A comparison of half-bridge resonant converter topologies," *IEEE Trans. Power Electron.*, vol. 3, 1988.

[16] S. Li and C. C. Mi, "Wireless power transfer for electric vehicle applications," *IEEE Journal of Emerging and Selected Topics in Power Electronics*, vol. 3, no. 1, pp. 4–17, 2015.

[17] PREMO. Wc-rx-002-90k receiving antenna flexible-pad for the wireless power transfer in the electric vehicles.

[18] J. W. Kolar, J. Biela, and J. Minibock, "Exploring the pareto front of multi-objective single-phase pfc rectifier design optimization - 99.2% efficiency vs. 7kw/din^3 power density," in *2009 IEEE 6th International Power Electronics and Motion Control Conference*, 2009, pp. 1–21.

[19] J. P. M. Figueiredo, F. L. Tofoli, and B. L. A. Silva, "A review of single-phase pfc topologies based on the boost converter," in *2010 9th IEEE/IAS International Conference on Industry Applications - INDUSCON 2010*, 2010, pp. 1–6.